J Mol Model (2009) 15:1281–1290
DOI 10.1007/s00894-009-0492-3

ORIGINAL PAPER

Theoretical modeling and experimental studies on N-n-Decyl-2-oxo-5-nitro-1-benzylidene-methylamine

Hasan Tanak · Ferda Erşahin · Yavuz Köysal · Erbil Ağar · Şamil Işık · Metin Yavuz

Received: 13 January 2009 / Accepted: 17 February 2009 / Published online: 31 March 2009

Abstract The Schiff base compound, N-n-Decyl-2-oxo-5-nitro-1-benzylidene-methylamine, has been -synthesized and characterized by IR, electronic spectroscopy, and X-ray single-crystal determination. Molecular geometry from X-ray experiment of the title compound in the ground state have been compared using the Hartree-Fock (HF) and density functional method (B3LYP) with 6-31G(d) basis set. Calculated results show that density functional theory (DFT) at B3LYP/6-31G(d) level can well reproduce the structure of the title compound. To investigate the solvent effect for the atomic charge distributions of the title compound, self-consistent reaction field theory with Onsager reaction field model was used. In addition, DFT calculations of the title compound, molecular electrostatic potential and thermodynamic properties were performed at B3LYP/6-31G(d) level of theory.

H. Tanak (✉) · Ş. Işık · M. Yavuz
Department of Physics, Faculty of Arts and Sciences,
Ondokuz Mayıs University,
55139 Kurupelit,
Samsun, Turkey
e-mail: htanak@omu.edu.tr

F. Erşahin
Gerze Sinop Vocational School, Sinop University,
Sinop, Turkey

Y. Köysal
Samsun Vocational School, Ondokuz Mayıs University,
55139 Kurupelit,
Samsun, Turkey

E. Ağar
Department of Chemistry, Faculty of Arts and Sciences,
Ondokuz Mayıs University,
55139 Kurupelit,
Samsun, Turkey

Keywords Density functional theory · Hartree-Fock · Electronic absorption spectra · Molecular electrostatic potential · Schiff base · Vibrational assignment

Introduction

By means of increasing development of computational chemistry in the past decade, the research of theoretical modeling of drug design, functional material design, etc., has become much more mature than ever. Many important chemical and physical properties of biological and chemical systems can be predicted from the first principles by various computational techniques [1]. In recent years, density functional theory (DFT) has been a shooting star in theoretical modeling. The development of better and better exchange-correlation functionals made it possible to calculate many molecular properties with comparable accuracies to traditional correlated *ab initio* methods, with more favorable computational costs [2]. Literature survey revealed that the DFT has a great accuracy in reproducing the experimental values of in geometry, dipole moment, vibrational frequency, etc. [3–9].

Schiff bases are used as starting materials in the synthesis of important drugs, such as antibiotics and antiallergic, antiphlogistic, and antitumor substances [10–12]. They are also used as components of rubber compounds [13]. Schiff bases have also been employed as ligands for the complexation of metal ions [14]. There are two characteristic properties of Schiff bases, *viz*. photochromism and thermochromism [15]. These properties result from proton transfer from the hydroxyl O atom to the imine N atom [16, 17]. In general, Schiff bases display two possible tautomeric forms, the phenol-imine (OH) and the keto-amine (NH) forms. Depending on the tautomers,

two types of intramolecular hydrogen bonds are observed in Schiff bases: O-H···N in phenol-imine [18, 19] and N-H···O in keto-amine [20–22] tautomers.

In this paper, we wish to report the synthesis, characterization and crystal structure of the Schiff base, N-n-Decyl-2-oxo-5-nitro-1-benzylidene-methylamine (Fig. 1), as well as the theoretical studies on it by using HF/6-31G(d) and DFT/B3LYP/6-31G(d) methods. The properties of the structural geometry, electronic charge distribution, molecular electrostatic potential (MEP) and the thermodynamic properties for the title compound at the B3LYP/6-31G(d) level were studied. We also make comparisons between experiments and calculations.

Experimental

The compound N-n-Decyl-2-oxo-5-nitro-1-benzylidene-methylamine was prepared by reflux a mixture of a solution containing 2-Hydroxy-5-nitrobenzaldehyde(0.025 g 0.15 mmol) in 20 ml ethanol and a solution containing Decylamine (0.0236 g 0.15 mmol) in 20 ml ethanol. The reaction mixture was stirred for 1 h under reflux. The crystals of N-n-Decyl-2-oxo-5-nitro-1-benzylidene-methylamine suitable for X-ray analysis were obtained from ethylalcohol by slow evaporation (yield % 65; m.p.371-373 K). The IR spectra were recorded in the 4000-400cm^{-1} region using KBr pellets on a Schmadzu FTIR-8900 spectrophotometer. Electronic absorption spectra were measured on a Unicam UV-VIS spectrophotometer in DMF.

Crystal data for the title compound

CCDC 710062, $C_{17}H_{26}N_2O_3$, M_w=306.40, triclinic, space group P −1; Z=2, a=5.4032(3) Å, b=8.3939(5) Å, c=19.2767(11) Å, α=83.817(5)°, β=84.576(5)°, γ=86.194(5)° and V=863.90(9) Å^3, F(000) = 332, D_x=1.178 g cm^{-3}. Full crystallographic data are available as supplementary material.

Computational methods

The molecular geometry is directly taken from the X-ray diffraction experimental result without any constrained. In the next step, the DFT calculations with a hybrid Functional B3LYP (Becke's Three parameter Hybrid Functional Using the LYP Correlation Functional) at 6-31G(d) basis set and the Hartree-Fock calculations at 6-31G(d) basis set by the Berny method [23, 24] were performed with the Gaussian 03 software package [25], and Gauss-view visualization program [26]. In order to evaluate the energetic and atomic charge behavior of the title compound in solvent, we carried out optimization calculations in the three kinds of solvent (chloroform, ethanol and water). The methodology used in this investigation is centered on Onsager's reaction field theory [27]. The simplest self-consistent reaction field model is the Onsager reaction field model. In this method, the solute occupies a fixed spherical cavity of radius a_0 within the solvent field. A dipole in the molecule will induce a dipole in the polar medium, and the electric field applied by the solvent dipole will in turn interact with the molecular dipole, leading to net stabilization. The systems with zero dipole moment will not exhibit a solvent effect for Onsager's model, and therefore, the calculations will give similar results for the gas phase. This is an inherent limitation of this method.

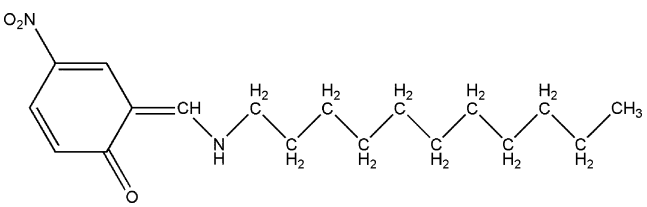

Fig. 1 Chemical diagram of the title compound $C_{17}H_{26}N_2O_3$

To investigate the reactive sites of the title compound the molecular electrostatic potential were evaluated using B3LYP/6-31G(d) method. Molecular electrostatic potential, *V(r),* at a given point *r(x, y, z)* in the vicinity of a molecule, is defined in terms of the interaction energy between the electrical charge generated from the molecule electrons and nuclei and a positive test charge (a proton) located at *r*. For the system studied the *V(r)* values were calculated as described previously using the equation [28],

$$V(r) = \sum Z_A \Big/ |R_A - r| - \int \rho(r') \Big/ |r' - r| \, d^3r' \qquad (1)$$

where Z_A is the charge of nucleus A, located at R_A, $\rho(r')$ is the electronic density function of the molecule, and r' is the dummy integration variable.

The thermodynamic properties of the title compound at different temperatures were calculated on the basis of vibrational analyses. In addition, electronic absorption spectra were calculated using the time-dependent density functional theory (TD-DFT) and time-dependent Hartree-Fock (TD-HF) methods [29–32].

Results and discussion

IR spectroscopy

Harmonic vibrational frequencies of the title compound were calculated by using DFT and HF method with 6-31G(d) basis set and the obtained frequencies were scaled by 0.9613 and 0.8929 [33], respectively. By using Gauss-View molecular visualization program [26], the vibrational bands

assignments have been made. In order to facilitate assignment of the observed peaks we have analyzed some vibrational frequencies and compared our calculation of the title compound with their experimental results and shown in Table 1.

The experimental N-H stretching modes were observed at 3352-3212 cm^{-1}, that have been calculated with B3LYP and HF at 2958.16 and 3271,33 cm^{-1}, respectively. As can be easily seen the experimental value of N-H stretching mode is closer to HF value than that of B3LYP. The C-H aromatic stretching mode was observed to be 3085 cm^{-1} experimentally, while that have been calculated at 3093.47 cm^{-1} for B3LYP and 3062.18 cm^{-1} for HF, respectively. The stretching C = O vibration gives rise to a band in the infrared experimental spectrum at 1672 cm^{-1}, while the calculated value for HF is predicted 8 cm^{-1} higher, at 1680 cm^{-1} and for B3LYP is predicted 48 cm^{-1} lower, at 1624 cm^{-1}. The experimental NO_2 asymmetric stretching mode appeared at 1545 cm^{-1} has been calculated at 1629.6 cm^{-1} and 1572.7 cm^{-1} for HF and B3LYP, respectively. The other calculated vibrational frequencies can be seen in Table 1. To make a comparison with the experimental observation, we present correlation graphics in Fig. 2 based on the calculations. As we can see from correlation graphics in Fig. 2 experimental fundamentals are found to have a good correlation with HF than DFT. Besides, the vibrational frequencies calculated by DFT method are more compatible to experimental values with the exception of N-H stretching mode which has the correlation coefficient R^2=0.99799.

Crystal structure

The structure of the title compound, $C_{17}H_{26}N_2O_3$, reveal that the nitrocyclohexa-2,4-dienone fragment is nearly planar, with the maximum deviation from the planarity 0.61(5) Å for atom C17. The nitrocyclohexa ring is twisted out of plane relative to the 2, 4-dienone moiety by 9.4(4)° in the compound.

The NH groups forms inter and intramolecular hydrogen bond with the carbonyl O atom. The hydrogen atom H11 is localized at N2. This is a verification of the preference for the keto-amine form in solid state. The presence of a quinoidal structure is further supported by the shortening of the bond O1-C5 to 1.2571(15) Å and the lengthening of the adjacent C-C bond in the phenyl ring [C5-C6=1.4335(19) Å and C4-C5=1.4434(16) Å], same conditions shown in the structure, 6-(2-Hydroxyanilinomethylene)-4-nitrocyclohexa-2, 4-dien-1-one [34]. And also these data show that there is significant elongation of the N2-C7 bond.

The title compound is stabilized by N-H···O type hydrogen bonds. There is a strong intramolecular N2-H11···O1 hydrogen bond (Fig. 3) with N2···O1 distance shorter than the sum of the van der Waals radii of O and N (3.07 Å) [35]. There is also a intermolecular hydrogen bond, namely, N2-H11···O1 (symmetry code: -x + 1, -y + 2, -z + 1). N-H···O type intermolecular hydrogen bonds held together $R_2^2(4)$ graph set [36] while N-H···O type intramolecular hydrogen bond bring into existence S(6) graph set by it self resulting in a network along the b axes shown in Fig. 4. There is also $N-O\cdots\pi$ interaction, namely, N1-O2·Cg(1) [Cg(1) is C1/C2/C3/C4/C5/C6], details of these bonds and interaction are given in Table 2.

Optimized geometry

B3LYP/6-31G(d) and HF/6-31G(d) calculations were performed on the title compound, respectively. Calculated geometric parameters are listed in Table 3 along with the

Table 1 Comparison of the experimental and calculated vibrational frequencies (cm^{-1})

Assignment [a]	Experiment	HF/6-31G(d)	B3LYP/6-31G(d)
ν(N-H)	3352-3212	3271.33	2958.16
ν_{ring}*(C-H)*	3085	3062.18	3093.47
ν(C-H)	2920-2856	2912.6-2836.12	2991.6-2894.4
ν(C = O)	1672	1680.27	1624.03
ν(NO_2)	1545	1629.6	1572.7
$\alpha(CH_2)$	1486	1481.5	1486
$\gamma_{ring}(CH)+\gamma(CH)+\gamma(CH_2)$	1466	1426.6	1434.9
ν(C-N)	1388	1436.57	1330.2
$\gamma_{ring}(CH)+\gamma(CH)+\gamma(NH)+\omega(CH_2)$	1320	1333.5	1326.7
$\omega(CH_2)$	1280	1276.2	1266.12
$\gamma_{ring}(CH)+\gamma(CH)$	1241	1214.1	1221.3
γ_{ring}*(CH)*	1104	1084.3	1112.3
ν (CH_2-CH_2)	1055	1066.01	1066.1
ω(NH) + ω(CH)	957	1041.8	1003.3
δ(NH) + δ(CH)	899	869.5	876.01

[a] *ν* = stretching, *α* = scissoring, *γ* = rocking, ω = wagging, δ = twisting

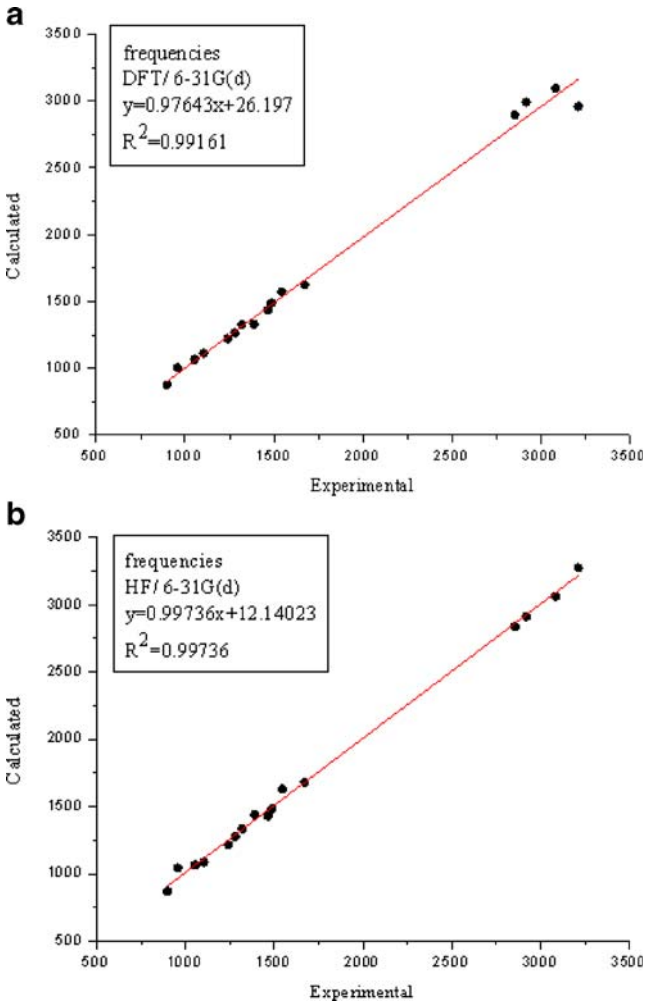

Fig. 2 Correlation graphics of calculated and experimental frequencies of the title compound

experimental data. When the X-ray structure of the title compound is compared with its optimized counterparts (see Fig. 5), conformational discrepancies are observed between them. The most remarkable discrepancies exist in the orientation of the decyl chain of the title compound. The conformation of the decyl chain is that most often found for larger alkanes, i.e., staggered with the largest substituents at any C-C bond anti to each other [37]. The largest deviation from the ideal 180° torsion angle is 7.47 (17)° for C8-C9-C10-C11. This torsion angle have been calculated as 180° for HF/6-31G(d) level and 179.2° for B3LYP/6-31G(d) level, respectively. The average C-C bond length in the chain is 1.507 (2) Å and the average C-C-C bond angle is 113.9 (1)° in X-ray structure, whereas the corresponding average values in optimized geometries are 1.529 Å and 112.9° for HF/6–31G(d), and 1.534 Å and 113.12° for B3LYP/6–31G(d). These values are similar to those found in related compounds already studied [1.516 (3) Å and 113.8 (8)° for 9-(n-dodecylaminomethyl) anthracene] [38] and [1.522 (2) Å and 113.29 (14)° for N-(n-Decyl)-4-nitroaniline] [39]. The zigzag decyl skeleton is less planar than in the above-mentioned compounds.

When the geometry of hydrogen bond in the optimized structures is examined, the proton donor group N2-H11 forms an intramolecular interaction with oxygen atom O1, with a bond length of 2.740 Å and a bond angle of 127.18° for HF and a bond length of 2.691 Å and a bond angle of 130.81° for B3LYP (Table 2). Similarly, an intermolecular H-bond, N2-H11···O1, of length 2.932 Å and bond angle 132.86° for HF and of length 2.908 Å and bond angle 129.53° for B3LYP is also observed. The presence of the H-bond appears as an important property of the molecule, stabilizing its conformation in the crystal; as shown in the Molecular modeling part, this is also visible in the model obtained for the molecule discussed [40]. In order to compare the theoretical results with the experimental values, root mean square error (RMSE) is used. Calculated RMSE for bond lengths and bond angles are 0.0223 Å and 1.0821° for B3LYP method, and 0.0217 Å and 1.1124° for HF method, respectively. These results show that B3LYP method gives better results for bond lengths on the contrary HF method is better in predicting the bond angles.

A logical method for globally comparing the structures obtained with the theoretical calculations is by superimposing the molecular skeleton with that obtained from X-ray diffraction, giving a RMSE of 0.40862 Å for B3LYP and 0.426234 Å for method HF (Fig. 5). According to these results, it may be concluded that the B3LYP calculation well reproduce the geometry of the title compound.

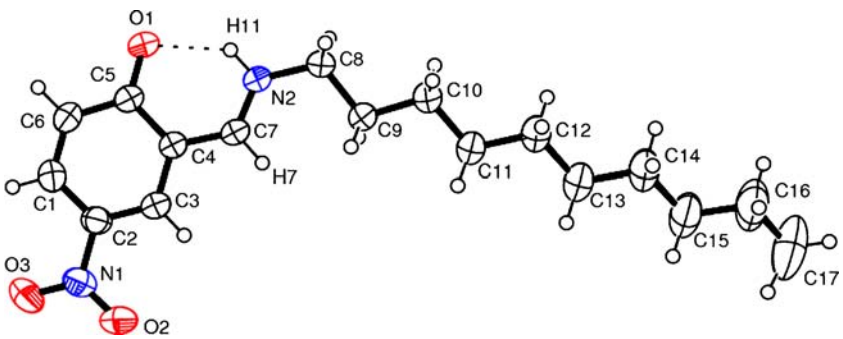

Fig. 3 Ortep 3 diagram of the title compound

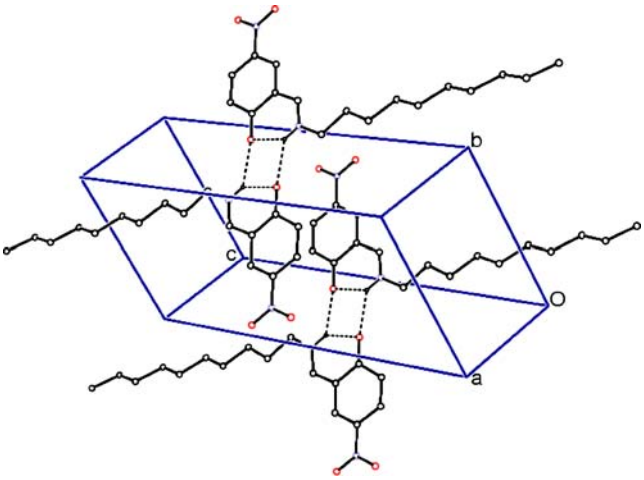

Fig. 4 Part of the crystal structure of the title compound showing the intra- and inter molecular N-H·O interactions as dashed lines. H atoms not involved in hydrogen bonding have been omitted for clarity

In spite of the some differences, calculated geometric parameters represent a good approximation and they are the bases for calculating other parameters, such as atomic charge distribution, electronic absorption spectra, molecular electrostatic potential (MEP) and thermodynamic properties, as we described below.

Atomic charge distributions in gas-phase and in solution-phase

The Mulliken atomic charges for the non-H atoms of the title compound calculated at HF/6-31G (d) and B3LYP/6-31G (d) level in gas-phase are presented in Table 4. To investigate the solvent effect for the atomic charge distributions of the title compound, based on B3LYP/6-311G(d) model and Onsager reaction field model, three kinds of solvent (chloroform, ethanol and water) were selected and calculated values were also listed in Table 4.

It can be seen from this table that the Mulliken atomic charges of the O1 atom and nitro group oxygen atoms (O2 and O3) have bigger negative atomic charges in gas phase. This behavior can be the result of electronegativity of nitro group and C5 = O1 double bond character. On the other hand, it can be found that in solution-phase, the atomic charge values of the O2 and O3 atoms are bigger than those in gas-phase and while their atomic charge values will increase with the increase of the polarity of the solvent, that value of O1 decrease with the increase of the solvent polarity. This result reveals that the coordinate ability of O1, O2 and O3 atoms will be changed in different solvents, which may be helpful when one wants to use the title compound to construct interesting metal complexes with different coordinate geometries [41]. This calculated result is not only consistent with many reported experimental facts [42–44], it also supports the original idea of our synthesis.

In addition, total energy and dipole moment have been calculated in both gas phase and solvent media with HF/6-31G (d) and B3LYP/6-31G (d) levels using Onsager reaction field model and the results are presented in Table 5. Looking at this table, we can conclude that obtained total energies of the title compound from both HF and DFT decreases with the increasing polarity of the solvent so that the stability of the title compound increases.

Electronic absorption spectra

The UV-visible spectrum of ortho hydroxylated Schiff bases which exist mainly as phenol-imine structure indicates the presence of a band at <400 nm, while compounds exist as keto-amine form show a new band, especially in polar and nonpolar solvents at >400 nm [45–54]. Experimentally, electronic absorption spectra of the title compound in DMF solvent show two bands at 360 and 406 nm, which correspond to phenol-imine and keto-amine forms, respectively. These values are similar to those found in related compounds [55]. According to experimental results,

Table 2 Hydrogen-bond geometry (Å, °)

D—H·A	D—H	H·A	D·A	D—H·A
X-ray				
N2-H11···O1	0.896(17)	1.960(17)	2.6762(14)	135.8(14)
N2-H11···O1^{i}	0.896(17)	2.204(16)	2.8843(13)	132.3(14)
N1-O2···Cg(1)^{ii}	4.55	3.5295(12)	4.010(13)	104.04(8)
B3LYP/6-31G(d)				
N2-H11···O1	1.031	1.901	2.691	130.81
N2-H11···O1^{i}	1.031	2.141	2.908	129.53
HF/6-31G(d)				
N2-H11···O1	1.007	2.011	2.740	127.18
N2-H11···O1^{i}	1.007	2.152	2.932	132.86

Symmetry codes: (i) –x + 1, -y + 2, -z + 1 (ii) -1 + x, y, **z**

Table 3 Selected molecular structure parameters

Parameters	Experimental	Calculated 6-31G(d)	
		HF	B3LYP
Bond lengths (Å)			
C2-N1	1.4391(16)	1.43573	1.45082
C4-C7	1.4228(18)	1.40050	1.41163
C5-O1	1.2571(15)	1.22490	1.26017
C7-N2	1.2863(16)	1.29923	1.31547
C8-N2	1.4669(16)	1.46002	1.46305
C8-C9	1.5088(17)	1.52390	1.52790
C9-C10	1.5213(19)	1.53147	1.53581
C10-C11	1.518(2)	1.52982	1.53445
C11-C12	1.507(2)	1.52978	1.53408
C12-C13	1.508(2)	1.52982	1.53433
C13-C14	1.502(3)	1.52983	1.53413
C14-C15	1.505(3)	1.52969	1.53410
C15-C16	1.501(3)	1.52979	1.53412
C16-C17	1.486(4)	1.52826	1.53207
N1-O3	1.2244(15)	1.19678	1.23536
N1-O2	1.2307(15)	1.20007	1.23662
RMSE		0.02230	0.0217
Bond angles (°)			
C3-C2-N1	119.18(11)	119.5589	119.3858
C1-C2-N1	119.77(12)	119.7156	119.5324
C3-C4-C7	117.81(11)	118.4294	119.1752
O1-C5-C6	122.38(11)	122.2158	122.2089
O1-C5-C4	121.54(12)	122.2199	121.9457
N2-C7-C4	124.56(11)	125.1046	122.7003
N2-C8-C9	114.66(10)	115.2434	115.4121
C8-C9-C10	111.15(11)	111.2472	111.4872
C11-C10-C9	112.31(12)	112.7622	113.0947
C12-C11-C10	114.70(14)	113.0434	113.1877
C11-C12-C13	113.94(16)	113.158	113.4877
C14-C13-C12	115.26(17)	113.2178	113.3972
C13-C14-C15	114.81(19)	113.2563	113.5782
C16-C15-C14	115.9(2)	113.3151	113.5186
C17-C16-C15	113.9(3)	113.0109	113.2411
O3-N1-O2	122.17(11)	123.917	124.0023
O3-N1-C2	118.95(11)	117.8039	117.7927
O2-N1-C2	118.88(11)	118.2791	118.2049
C7-N2-C8	126.09(10)	128.1971	127.8723
RMSE		1.0821	1.1124
Torsion angles (°)			
C1-C2-N1-O3	5.2(2)	0.0015	-0.0082
C4-C7-N2-C8	175.50(13)	180.00	179.42
C9-C8-N2-C7	6.6(2)	-0.0228	3.6822
N2-C8-C9-C10	-176.29(14)	180.00	179.62
C7-C4-C5-O1	2.7(2)	0.0004	0.0841
C8-C9-C10-C11	-172.53(17)	180.00	-179.20
C10-C11-C12-C13	-173.3(2)	-179.99	-179.03
C12-C13-C14-C15	-174.1(3)	-179.99	-179.28
C14-C15-C16-C17	-176.4(4)	179.99	-179.62

the keto-amine form is dominant in DMF solvent which has absorption band at 406 nm with log ε=4.704.

Electronic absorption spectra were calculated by TD-DFT and TD-HF methods based on the B3LYP/6-31G(d) and HF/6-31G(d) levels optimized structure, respectively. For TD-HF calculations, the predicted absorption wavelength is at 282.39 nm with oscillator strength being 0.3974. It is obvious that this band is not corresponding to the experimental results, which shows that to use the TD-HF method here to predict the electronic absorption spectra is not reasonable. For TD-DFT calculations, the theoretical absorption band is at 374 nm with the oscillator strength being 0.2012. That is, for the title compound, the TD-DFT method is convenient to predict the electronic absorption spectra. According to the TD-DFT calculational electronic absorption spectra show that the maximum absorption wavelength corresponding to the electronic transition from the highest occupied molecular orbital (HOMO) to the lowest unoccupied molecular orbital (LUMO). The frontier molecular orbitals (HOMO and LUMO) of the title compound are shown in Fig. 6. As seen from Fig. 6, both the highest occupied molecular orbitals (HOMO) and the lowest-lying unoccupied molecular orbitals (LUMO) are mainly localized nitrocyclohexa ring and N2-H11 bond.

Molecular orbital coefficients analyses based on optimized geometry indicate that, for the title compound, the frontier molecular orbitals are mainly composed of *p* atomic orbitals, so above electronic transitions are mainly derived from the contribution of bands $\pi \rightarrow \pi^*$.

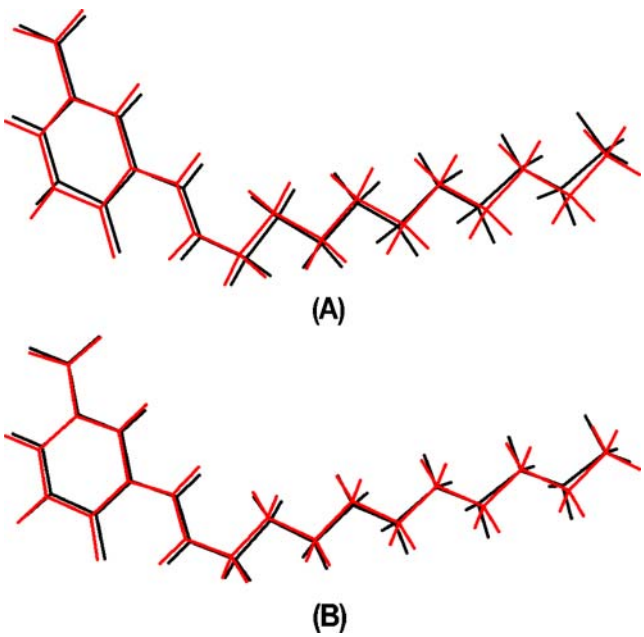

Fig. 5 Atom-by-atom superimposition of the structures calculated (red) (A = DFT; B = HF) over the X-ray structure (black) for the title compound

Table 4 Atomic charges (*e*) of the title compound in gas phase and solution phase

	In gas phase		In solution phase B3LYP/6-31G(d)		
	HF/6-31G(d)	B3LYP/6-31G(d)	Chloroform (ε=4.9)	Ethanol (ε=24.55)	Water (ε=78.39)
C1	0.139581	0.042200	0.025411	0.018343	0.016865
C2	0.075751	0.252783	0.252716	0.252790	0.252813
C3	0.148289	-0.036292	-0.033908	-0.032960	-0.032768
C4	-0.238609	0.025937	0.023733	0.023104	0.022962
C5	0.589348	0.426098	0.425991	0.425920	0.425905
C6	-0.086876	-0.048019	-0.055400	-0.058531	-0.059172
C7	0.474885	0.278395	0.291239	0.296548	0.297657
C8	0.324245	0.234248	0.245066	0.249710	0.250650
C9	-0.017892	0.012821	0.006523	0.003808	0.003265
C10	0.018506	0.017258	0.027117	0.031304	0.032165
C11	0.010977	0.010357	0.002815	-0.000338	-0.000984
C12	0.005864	0.005767	0.014852	0.018662	0.019439
C13	0.004556	0.004472	-0.003378	-0.006642	-0.007309
C14	0.002256	0.002443	0.011580	0.015400	0.016179
C15	0.003637	0.008478	0.000421	-0.002915	-0.003591
C16	0.005017	0.013591	0.023576	0.027749	0.028596
C17	-0.002171	-0.015004	-0.006230	-0.002336	-0.001481
N1	0.519860	0.367563	0.360154	0.356853	0.356153
N2	-0.286297	-0.159891	-0.150544	-0.146627	-0.145766
O1	-0.704510	-0.609200	-0.603262	-0.600451	-0.599861
O2	-0.505018	-0.423234	-0.427435	-0.429444	-0.429881
O3	-0.481399	-0.410771	-0.431036	-0.439946	-0.441836

Molecular electrostatic potential

Molecular electrostatic potential (MEP) is related to the electronic density and is a very useful descriptor in understanding sites for electrophilic attack and nucleophilic reactions as well as hydrogen bonding interactions [56–58]. The electrostatic potential $V(r)$ are also well suited for analyzing processes based on the "recognition" of one molecule by another, as in drug-receptor, and enzyme-substrate interactions, because it is through their potentials that the two species first "see" each other [59, 60]. Being a real physical property $V(r)s$ can be determined experimentally by diffraction or by computational methods [61].

To predict reactive sites for electrophilic and nucleophilic attack for the title molecule, MEP was calculated at the B3LYP/6-31G(d) optimized geometry. The negative (red color) regions of MEP were related to electrophilic reactivity and the positive (blue color) ones to nucleophilic reactivity shown in Fig. 7.

As easily can be seen in Fig. 7, this molecule has two possible sites for electrophilic attack. The negative regions are mainly over the O1 atom and between O2 and O3 atoms. The most negative V(r) value is associated with the region between O2 and O3 atoms with a value -0.059 a.u. while the O1 value is about -0.050 a.u. Thus, the calculations suggested that the preferred site for electrophilic attack is the region between O2 and O3 atoms, followed from the O1 atom. A maximum positive region is localized on the C7-H7 bond with a value of +0.044 au indicating a possible site for nucleophilic attack.

Table 5 Total energies and dipole moments of the title compound in different solvent

	HF/6-31G(d)		B3LYP/6-31G(d)	
Solvent	Energy (a.u.)	μ (Debyes)	Energy (a.u.)	μ (Debyes)
Gas	-992.2694571	9.2783	-998.56715044	8.9146
Chloroform	-992.2744082	11.6871	-998.57182112	11.4750
Ethanol	-992.2764519	12.6884	-998.57381087	12.5871
Water	-992.2768750	12.8980	-998.57422813	12.8219

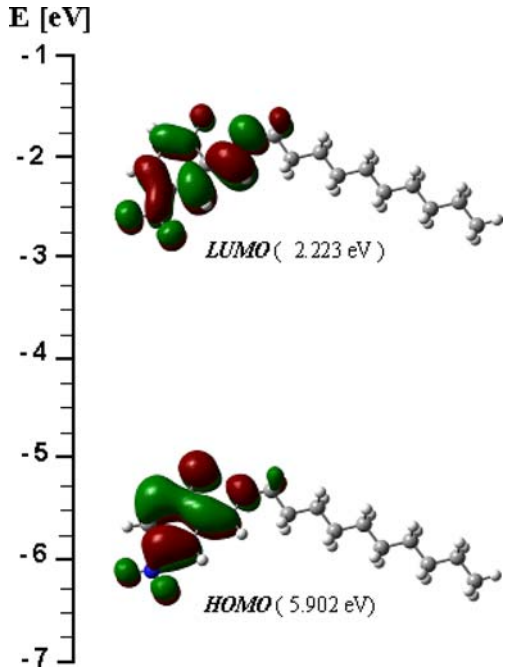

Fig. 6 *HOMO* and *LUMO* of the title compound

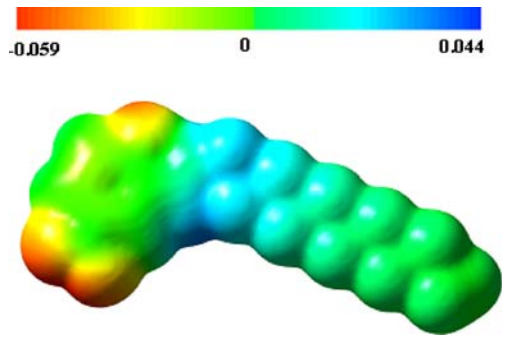

Fig. 7 Molecular electrostatic potential map calculated at B3LYP/6-31G(d) level

Table 6 Thermodynamic properties at different temperatures at B3LYP/6-31G(d,p) level

T (K)	$H_m^0\,(kcal.mol^{-1})$	$C_{p,m}^0\,(cal.mol^{-1}.K^{-1})$	$S_m^0(cal.mol^{-1}.K^{-1})$
200	3.165	63.525	145.589
250	6.742	75.772	161.503
298.15	10.787	88.377	176.269
300	10.955	88.870	176.830
350	15.831	102.186	191.837
400	21.365	115.114	206.598
450	27.528	127.269	221.101
500	34.275	138.480	235.309

Thermodynamic properties

On the basis of vibrational analysis and statistical thermodynamics, the standard thermodynamic functions: heat capacity $\left(C^0_{p,m}\right)$, entropy $\left(S^0_m\right)$, and enthalpy $\left(H^0_m\right)$ were obtained at B3LYP/6-31G(d) level and listed in Table 6.

Table 6 shows that the standard heat capacities, entropies, and enthalpies increase at any temperature from 200.00 to 500.00 K, because the intensities of molecular vibration increase with the increasing temperature.

The correlations between these thermodynamic properties and temperatures T are shown in Fig. 8. The correlation equations are as follows:

$$C^0_{p,m} = 7.79777 + 0.28511\,T - 4.55787 \times 10^{-5}\ \left(R^2 = 0.99955\right) \quad (2)$$

$$S^0_m = 79.64065 + 0.34278\,T - 6.30643 \times 10^{-5}\,T^2\ \left(R^2 = 0.99999\right) \quad (3)$$

$$H^0_m = -4.77016 + 0.01395\,T + 1.28357 \times 10^{-4}\,T^2\ \left(R^2 = 1\right) \quad (4)$$

These equations will be helpful for the further studies of the title compound.

Conclusions

N-n-Decyl-2-oxo-5-nitro-1-benzylidene-methylamine has been synthesized and characterized by IR, UV–Vis, and X-ray single-crystal diffraction. The comparisons between the calculated results and the X-ray experimental data indicate B3LYP/6-31G(d) method is better than HF/6-31G(d) method in evaluating geometrical parameters. For the calculation of vibrational frequencies both the methods B3LYP/6-31G(d) and HF/6- 31G(d) can predict the IR spectrum of title compound well.

The carbonyl oxygen atom has bigger negative atomic charge in gas phase and its atomic charge value will decrease with the increase of the polarity of the solvent. Molecular electrostatic potential map shows several possible sites for electrophilic attack. Molecular orbital coefficients analyses suggest that the electronic spectra is corresponding to $\pi \rightarrow \pi^*$ electronic transition. The correlations between the thermodynamic properties $C^o_{p,m}$, S^o_m, H^o_m and temperatures T are also obtained.

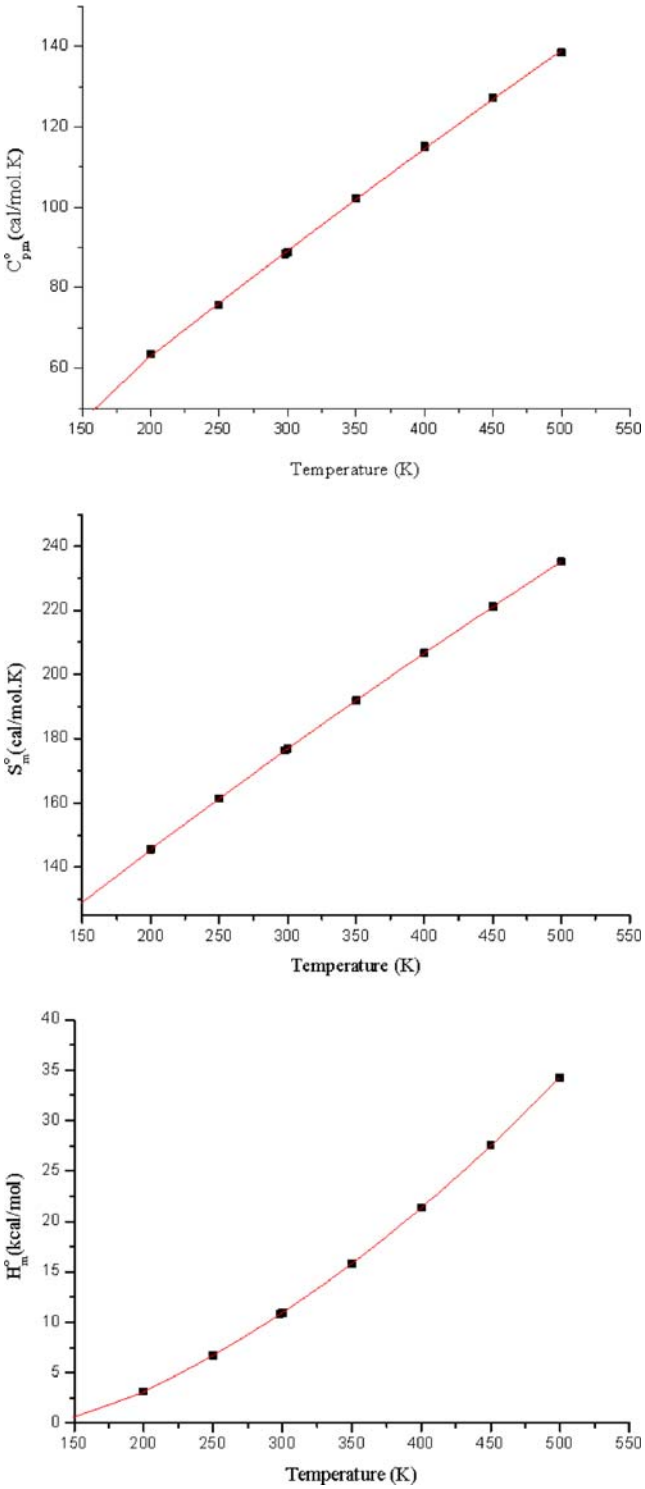

Fig. 8 Correlation graphics of thermodynamic properties and temperatures

Acknowledgments This study was supported financially by the Research Centre of Ondokuz Mayıs University (Project No: F-476).

References

1. Zhang Y, Guo ZJ, You XZ (2001) J Am Chem Soc 123:9378–9387
2. Proft FD, Geerlings P (2001) Chem Rev 101:1451–1464
3. Fitzgerald G, Andzelm J (1991) J Phys Chem 95:10531–10534
4. Ziegler T (1991) Pure Appl Chem 63:873–878
5. Andzelm J, Wimmer E (1992) J Chem Phys 95:1208–1303
6. Scuseria GE (1992) J Chem Phys 97:7528–7530
7. Dickson RM, Becke AD (1993) J Chem Phys 99:3898–3905
8. Johnson BG, Gill PMW, Pople JA (1993) J Chem Phys 98:5612–5626
9. Oliphant N, Bartlett RJ (1994) J Chem Phys 100:6550–6561
10. Barton D, Ollis WD (1979) Comprehensive organic chemistry, vol 2. Pergamon, Oxford
11. Layer RW (1963) Chem Rev 63:487–510
12. Ingold CK (1969) Structure and mechanism in organic chemistry, 2nd edn. Cornell Univ, Ithaca
13. Novopol'tseva OM (1995) Cand Sci (Chem), Dissertation, Volgograd
14. Aydoğan F, Öcal N, Turgut Z, Yolaçan C (2001) Bull Korean Chem Soc 22:476–480
15. Cohen MD, Schmidt GMJ, Flavian S (1964) J Chem Soc 2041-2051
16. Hadjoudis E, Vitterakis M, Mavridis IM (1987) Tetrahedron 43:1345–1360
17. Xu XX, You XZ, Sun ZF, Wang X, Liu HX (1994) Acta Crystallogr C50:1169–1171
18. Petek H, Albayrak Ç, Ağar E, Ocak İskeleli N, Şenel I (2007) Acta Cryst E63:810–812
19. Özek A, Albayrak Ç, Odabaşoğlu M, Büyükgüngör O (2007) Acta Cryst C63:177–180
20. Karabıyık H, Ocak İskeleli N, Petek H, Albayrak Ç, Ağar E (2008) J Mol Struct 873:130–136
21. Koşar B, Büyükgüngör O, Albayrak Ç, Odabaşoğlu M (2004) Acta Cryst C60:458–460
22. Tanak H, Erşahin F, Ağar E, Büyükgüngör O, Yavuz M (2008) Anal Sci 24:237–238
23. Schlegel HB (1982) J Comput Chem 3:214–218
24. Peng C, Ayala PY, Schlegel HB, Frisch MJ (1996) J Comput Chem 17:49–56
25. Frisch MJ, Trucks GW, Schlegel HB, Scuseria GE, Robb MA, Cheeseman JR, Montgomery JA Jr, Vreven T, Kudin KN, Burant JC, Millam JM, Iyengar SS, Tomasi J, Barone V, Mennucci B, Cossi M, Scalmani G, Rega N, Petersson GA, Nakatsuji H, Hada M, Ehara M, Toyota K, Fukuda R, Hasegawa J, Ishida M, Nakajima T, Honda Y, Kitao O, Nakai H, Klene M, Li X, Knox JE, Hratchian HP, Cross JB, Bakken V, Adamo C, Jaramillo J, Gomperts R, Stratmann RE, Yazyev O, Austin AJ, Cammi R, Pomelli C, Ochterski JW, Ayala PY, Morokuma K, Voth GA, Salvador P, Dannenberg JJ, Zakrzewski VG, Dapprich S, Daniels AD, Strain MC, Farkas O, Malick DK, Rabuck AD, Raghavachari K, Foresman JB, Ortiz JV, Cui Q, Baboul AG, Clifford S, Cioslowski J, Stefanov BB, Liu G, Liashenko A, Piskorz P, Komaromi I, Martin RL, Fox DJ, Keith T, Al-Laham MA, Peng CY, Nanayakkara A, Challacombe M, Gill PMW, Johnson B, Chen W, Wong MW, Gonzalez C, Pople JA (2004) Gaussian 03, Revision E.01. Gaussian Inc, Wallingford CT
26. Frisch A, Dennington II R, Keith T, Millam J, Nielsen AB, Holder AJ, Hiscocks J (2007) GaussView Reference, Version 4.0. Gaussian Inc, Pittsburgh
27. Onsager L (1936) J Am Chem Soc 58:1486–1493
28. Politzer P, Murray J (2002) Theor Chem Acc 108:134–142
29. Runge E, Gross EKU (1984) Phys Rev Lett 52:997–1000
30. Stratmann RE, Scuseria GE, Frisch MJ (1998) J Chem Phys 109:8218–8224
31. Bauernschmitt R, Ahlrichs R (1996) Chem Phys Lett 256:454–464
32. Casida ME, Jamorski C, Casida KC, Salahub DR (1998) J Chem Phys 108:4439–4449
33. Foresman JB, Frisch A (1996) Exploring chemistry with electronic structure methods, 2nd edn. Gaussian Inc, Pittsburgh, PA
34. Böhme U, Fels S (2008) Acta Cryst E64:178
35. Bondi A (1964) J Phys Chem 68:441–450
36. Bernstein J, Davies RE, Simoni L, Chang NL (1995) Angew Chem Int Ed Engl 34:1555–1573
37. Ramos Silva M, Matos Beja A, Paixao JA, Sobral AJFN, Lopesb SHA, Rocha Gonsalves AMd'A (2002) Acta Cryst C58:572-574
38. Ramos Silva M, Matos Beja A, Paixao JA, Alte da Veiga L, Sobral AJFN, Rebanda NGCL, Rocha Gonsalves AMd'A (2000) Acta Cryst C56:1136-1138
39. Yonkey MM, Walczak CP, Squattrito PJ, Mohantya DK, Kirschbaum K (2008) Acta Cryst E64:549
40. Jezierska A, Jerzykiewicz LB, Kołodziejczak J, Sobczak JM (2007) J Mol Struct 839:33–40
41. Jian FF, Zhao PS, Bai ZS, Zhang L (2005) Struct Chem 16:635–639
42. Baldini M, Belicchi-Ferrari M, Bisceglie F, Pelosi G, Pinelli S, Tarasconi P (2003) Inorg Chem 42:2049–2055
43. Ashfield LJ, Cowley AR, Dilworth JR, Donnelly PS (2004) Inorg Chem 43:4121–4123
44. Casas JS, Castellano EE, Ellena J, Garcia Tasende MS, Sanchez A, Sordo J, Vidarte MJ (2003) Inorg Chem 42:2584–2595
45. Ledbetter JW Jr (1968) J Phys Chem 72:4111–4115
46. Dudek GO, Dudek EP (1966) J Am Chem Soc 88:2407–2412
47. Salman SR, Shawkat SH, Al-Obaidi GM (1990) Can J Spectros 35:25–27
48. Salman SR, Shawkat SH, Al-Obaidi GM (1989) Spectrosc Lett 22:1265–1273
49. Yıldız M, Kılıç Z, Hökelek T (1998) J Mol Struct 441:1–10
50. Nazır H, Yıldız M, Yılmaz H, Tahir MN, Ülkü D (2000) J Mol Struct 524:241–250
51. Ünver H, Yıldız M, Zengin DM, Özbey S, Kendi E (2001) J Chem Crystallogr 31:211–216
52. Salman SR, Kamounah FS (2002) Spectrosc Lett 35:327–335
53. Yıldız M (2004) Spectrosc Lett 37:367–381
54. Ünver H, Yıldız M, Kiraz A, Özgen Ö (2009) J Chem Crystallogr 39:17-23
55. Alarcon SH, Pagani D, Bacigalupo J, Olivieri AC (1999) J Mol Struct 475:233–240
56. Scrocco E, Tomasi J (1978) Adv Quantum Chem 11:115–121
57. Luque FJ, Lopez JM, Orozco M (2000) Theor Chem Acc 103:343–345
58. Okulik N, Jubert AH (2005) Internet Electron J Mol Des 4:17–30
59. Politzer P, Laurence PR, Jayasuriya K, McKinney J (1985) Special issue of Environ Health Perspect 61:191–202
60. Scrocco E, Tomasi J (1973) Topics in current chemistry, vol. 7. Springer, Berlin, p 95
61. Politzer P, Truhlar DG (1981) Chemical applications of atomic and molecular electrostatic potentials. Plenum, New York